

# Loss of Function in Phenylketonuria Is Caused by Impaired Molecular Motions and Conformational Instability

Søren W. Gersting,<sup>1</sup> Kristina F. Kemter,<sup>1</sup> Michael Staudigl,<sup>1</sup> Dunja D. Messing,<sup>1</sup> Marta K. Danecka,<sup>1</sup> Florian B. Lagler,<sup>2</sup> Christian P. Sommerhoff,<sup>3</sup> Adelbert A. Roscher,<sup>1</sup> and Ania C. Muntau<sup>1,\*</sup>

A significant share of patients with phenylalanine hydroxylase (PAH) deficiency benefits from pharmacological doses of tetrahydrobiopterin (BH<sub>4</sub>), the natural PAH cofactor. Phenylketonuria (PKU) is hypothesized to be a conformational disease, with loss of function due to protein destabilization, and the restoration of enzyme function that is observed in BH<sub>4</sub> treatment might be transmitted by correction of protein misfolding. To elucidate the molecular basis of functional impairment in PAH deficiency, we investigated the impact of ten *PAH* gene mutations identified in patients with BH<sub>4</sub>-responsiveness on enzyme kinetics, stability, and conformation of the protein (F55L, I65S, H170Q, P275L, A300S, S310Y, P314S, R408W, Y414C, Y417H). Residual enzyme activity was generally high, but allostery was disturbed in almost all cases and pointed to altered protein conformation. This was confirmed by reduced proteolytic stability, impaired tetramer assembly or aggregation, increased hydrophobicity, and accelerated thermal unfolding—with particular impact on the regulatory domain—observed in most variants. Three-dimensional modeling revealed the involvement of functionally relevant amino acid networks that may communicate misfolding throughout the protein. Our results substantiate the view that PAH deficiency is a protein-misfolding disease in which global conformational changes hinder molecular motions essential for physiological enzyme function. Thus, PKU has evolved from a model of a genetic disease that leads to severe neurological impairment to a model of a treatable protein-folding disease with loss of function.

## Introduction

Deficiency of phenylalanine hydroxylase (PAH; EC 1.14.16.1) causes phenylketonuria (PKU [MIM 261600]) and is the most common inborn error of amino acid metabolism in European-descended populations. Since the introduction of a dietary treatment fifty years ago, PKU has been the prototype for a treatable genetic disease and, later, for genetic screening in human populations.<sup>1</sup> The recent recognition of a new pharmacologically treatable phenotype of PAH deficiency challenged the classical view of hereditary diseases that result in loss of enzyme function. We previously showed that a significant share of PKU patients responds to oral administration of the natural PAH cofactor (tetrahydrobiopterin, BH<sub>4</sub>) although these individuals do not display biochemical evidence of BH<sub>4</sub> deficiency. The treatment reduces blood phenylalanine concentrations, restores enzyme activity in vivo, and significantly increases dietary-protein tolerance.<sup>2</sup> Some authors proposed that restoration of enzyme function observed under treatment with pharmacological doses of BH<sub>4</sub> is transmitted by correction of PAH misfolding.<sup>2–5</sup>

About 80% of all mutations in the *PAH* gene are missense, and experimental data on the conformational impact of single amino acid replacements on allostery, stability, and folding of the PAH protein is scarce. Because the crystal structure of full-length PAH has not yet been completely solved,<sup>6–8</sup> a composite model is commonly used

for 3D structural analysis.<sup>9</sup> PAH is a homotetrameric enzyme, with each subunit composed of three functional domains: the N-terminal regulatory domain (residues 1–142); the catalytic domain (residues 143–410), which includes binding sites for substrate and cofactor; and the oligomerization domain at the C terminus (residues 411–452). There is a high degree of structural interplay between the single domains and the subunits, respectively.<sup>6–8,10–13</sup> Substrate (L-phenylalanine) and cofactor binding induce conformational changes, which are transmitted through networks of side-chain interactions.<sup>14,15</sup> This is the basis for homotropic allostery that allows for fine-tuned regulation of PAH enzyme activity comprising substrate activation, modulation of oligomerization, and the affinity to substrate and cofactor.<sup>3,4,12,15</sup> We hypothesized that the structural flexibility of PAH permits gross conformational changes required for enzyme function and thus renders the enzyme susceptible to protein misfolding. This view was supported by previous studies demonstrating disturbed oligomerization and accelerated degradation of some variant PAH proteins.<sup>3,4,16–19</sup> However, only little is known about the structural mechanisms leading to loss of function in phenylketonuria and in other inherited diseases that exhibit loss-of-function pathogenesis.

The aim of this study, therefore, was to elucidate the molecular basis of loss of function in PKU. The impact of single side-chain replacements associated with BH<sub>4</sub>-responsiveness on function and conformational stability of

<sup>1</sup>Department of Molecular Pediatrics, Children's Research Center, Dr. von Hauner Children's Hospital, Ludwig Maximilians University, 80337 Munich, Germany; <sup>2</sup>Department of Medical Genetics, Molecular and Clinical Pharmacology, Innsbruck Medical University, 6020 Innsbruck, Austria; <sup>3</sup>Department of Clinical Chemistry and Clinical Biochemistry, Surgical Clinic, Ludwig Maximilians University, 80337 Munich, Germany

\*Correspondence: [ania.muntau@med.uni-muenchen.de](mailto:ania.muntau@med.uni-muenchen.de)

DOI 10.1016/j.ajhg.2008.05.013. ©2008 by The American Society of Human Genetics. All rights reserved.

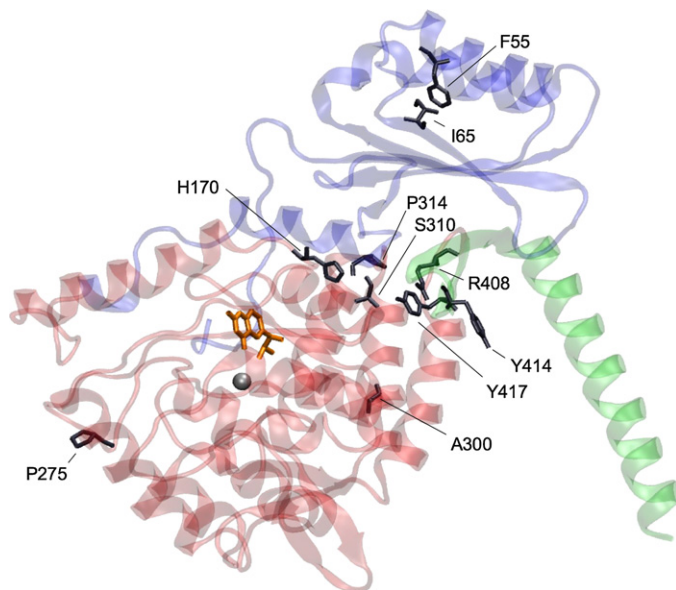


**Figure 1. Structural Localization of PAH Missense Mutations Analyzed**

The PAH monomer, shown as a ribbon representation, is composed of three functional domains: the N-terminal regulatory domain (residues 19–142, blue), the central catalytic domain (residues 143–410, red), and the C-terminal oligomerization domain (residues 411–452, green). The active-site iron (silver sphere) and the cofactor (orange stick model) are shown. Amino acid residues affected by mutations are shown as stick models.

the PAH protein was analyzed on the basis of enzyme kinetics, oligomerization, limited proteolysis, thermal inactivation, thermal unfolding, and 3D structural modeling. The mutations analyzed in this study caused pleiotropic effects. Residual enzyme activity was generally high, but allostery was disturbed in almost all cases and pointed to altered protein conformation. Reduced proteolytic stability of most variants, impaired tetramer assembly or aggregation, increased hydrophobicity, and accelerated thermal unfolding with particular impact on the regulatory domain corroborated the hypothesis of protein misfolding. To explain the remote effects on structure and function that were observed, we propose a model of protein misfolding as communicated throughout the protein by disruption of functional networks due to single amino acid replacements.

In the past twenty years, scientists have made significant efforts to identify a consistent relationship between the PAH genotype, in vitro residual enzyme activities, and the clinical phenotype.<sup>20–22</sup> A recent report from Pey and colleagues in this journal marked a breakthrough by opening the view on global conformation of PAH.<sup>23</sup> Using computational analyses, they predicted conclusive correlations between the mutational energetic impact on the protein and the clinical phenotype. Our results now provide experimental evidence and new insights into how PAH missense mutations induce conformational protein destabilization and loss of PAH function.

## Material and Methods

### Subjects and Mutations

In a previous study, we identified five unrelated patients bearing six mutations in the PAH gene that have not yet been characterized in vitro.<sup>2</sup> Three individuals were classified as having mild PKU (plasma phenylalanine concentrations in the absence of treatment exceeded 600  $\mu\text{mol/l}$  but do not reach values higher than 1200

$\mu\text{mol/l}$ ): patient 1, a Turkish girl born to consanguineous parents; patient 2, a German girl born to nonconsanguineous parents; and patient 5, a Turkish boy born to consanguineous parents. Patient 3, a German girl, and patient 4, a female German newborn, were classified as having mild hyperphenylalaninemia, with plasma phenylalanine concentrations consistently below 600  $\mu\text{mol/l}$  on an unrestricted diet. In all patients, hyperphenylalaninemia had been detected by newborn-screening programs, and BH<sub>4</sub>-responsiveness was subsequently demonstrated in an extended BH<sub>4</sub>-loading test.<sup>2</sup> BH<sub>4</sub> deficiency due to genetic disorders of biosynthesis or regeneration of the cofactor had been ruled out in all cases by the determination of urinary pterins and the activity of dihydropteridin reductase in erythrocytes. We obtained written informed consent for genotyping from the families. Mutations and clinical phenotypes of the individual patients are summarized in Table S1. The structural localization of mutations characterized in this study was mapped to the composite model of a PAH monomer (Figure 1). The mutations were located in the regulatory domain (F55L, I65S), in the catalytic domain (H170Q, P275L, A300S, S310Y, P314S, R408W), or in the dimerization motif of the oligomerization domain (Y414C, Y417H).

### Plasmid Constructs and Site-Directed Mutagenesis

The cDNA of human *phenylalanine hydroxylase* (EST clone obtained from imaGenes, formerly RZPD, Germany) was cloned into the pMAL-c2E expression vector (New England Biolabs) encoding an N-terminal MBP (maltose-binding protein) tag and an enterokinase cleavage site. PAH mutants were constructed with the use of the QuikChange site-directed mutagenesis kit (Stratagene). Authenticity of the mutagenesis was verified by DNA sequencing.

### Expression and Purification

Expression plasmids were transformed into *E. coli* DH5 $\alpha$ . Bacteria were grown to midexponential phase at 37°C, and overexpression of wild-type and variant MBP-PAH fusion proteins was induced with 0.3 mM isopropylthio- $\beta$ -D-galactoside (IPTG). MBP-PAH fusion proteins were more prone to form high-molecular-weight aggregates at two hours of induction than they were at longer induction periods, but the relative recovery of the tetrameric and the dimeric form was similar (own and previous observations<sup>24</sup>). To avoid artificial formation of aggregated PAH, we chose an induction time of 20 hr. Proteins were purified on ÄKTAexpress (GE Healthcare) at 4°C by affinity chromatography (amylose resin, New England Biolabs) as described previously,<sup>25</sup> followed by size-exclusion chromatography with a HiLoad 16/60 Superdex 200 column (GE Healthcare). The isolated tetrameric fusion proteins were collected, and protein concentrations were determined spectrophotometrically with the use of the absorption coefficient A<sub>280</sub>,<sup>25</sup> or the dye-binding Bradford assay.

It was previously shown that the MBP tag does not significantly affect PAH enzyme activity, kinetic parameters, or the oligomeric state of the protein.<sup>16,17,25–27</sup> Moreover, a comparative analysis of limited proteolysis, thermal inactivation, and thermal denaturation with the fusion protein and the cleaved PAH protein revealed no significant difference (data not shown).

### Analysis of Oligomerization

Oligomerization profiles were obtained by size-exclusion chromatography, and peaks corresponding to aggregated forms, tetramers, dimers, and monomers were determined with the use of LMW and HMW gel-filtration calibration kits (GE-Healthcare). Relative amounts of the different oligomeric states were calculated by deconvolution of the chromatograms with the use of the ACD/ChromManager software (Advanced Chemistry Development). Blue dextran was used for determination of the void volume ( $V_0$ , 45.3 ml).

### PAH-Activity Assay

PAH activity was determined as previously described.<sup>25,28</sup> Tetrameric wild-type or variant MBP-PAH (0.01 mg/ml) was preincubated with the L-phenylalanine (L-Phe) substrate for 5 min at 25°C in a standard reaction buffer containing 15 mM Na HEPES, pH 7.3 and 1 mg/ml catalase. After the addition of 10 μM ferrous ammonium sulfate and an additional incubation of 1 min, the reaction was initiated with BH<sub>4</sub> (6[R]-L-erythro-5,6,7,8-tetrahydrobiopterin, Cayman Chemicals) stabilized in 2 mM dithiothreitol (DTT). Kinetic parameters were determined at standard L-Phe concentration (1 mM) with variable cofactor concentrations (0–704.1 μM BH<sub>4</sub>) or at standard BH<sub>4</sub> concentration (75 μM) and variable L-Phe concentrations (0–1 mM), respectively. Because of early substrate inhibition, L-Phe concentrations were restricted to 0–250 μM for P314S and to 0–500 μM for Y414C and Y417H, respectively. To determine the level of substrate activation, a preincubation with the substrate was omitted and the reaction was triggered by simultaneous addition of 1 mM L-Phe and 75 μM BH<sub>4</sub>. All concentrations mentioned refer to the final concentration in a 100 μl reaction mixture. The amount of the L-tyrosin (L-Tyr) product formed after 1 min was measured by HPLC and assayed as triplicates. Steady-state kinetic parameters of three independent experiments were calculated by nonlinear regression analysis with the use of GraphPad Prism 4.0c (GraphPad Software). Enzyme kinetic parameters at variable substrate concentrations displayed cooperativity and were calculated with the Hill equation. Enzyme kinetic parameters at variable cofactor concentrations were calculated with the Michaelis-Menten equation or with the modified Michaelis-Menten equation<sup>29</sup> in the case of cofactor inhibition (WT, F55L, I65S, P314S, Y417H). All experimental data were confirmed by repeated analyses of different protein purifications.

### Limited Proteolysis by Proteinase K

The purified tetrameric MBP-PAH fusion proteins of wild-type PAH and its variant forms were digested with proteinase K at 37°C in a buffer containing 20 mM Na HEPES, 200 mM NaCl, and 38.4 mM DTT at pH 7.0. Stocks of proteinase K and MBP-PAH were prepared in 20 mM Na HEPES, 200 mM NaCl, pH 7.0 at final concentrations of 1 μg/ml and 1 mg/ml, respectively, and mixed at protease to substrate ratio of 1:5000 by weight. Proteolysis was terminated at 5, 10, 15, 20, 30, 60, 90, and 120 min time points by addition of the inhibitor phenylmethylsulphonyl fluoride (PMSF) at a final concentration of 4 mM. The reaction mixtures

were subjected to SDS-PAGE under reducing conditions with 4%–12% gradient polyacrylamide gels (Invitrogen). The pattern of proteolysis was monitored by immunoblotting. MBP-PAH fusion proteins and their proteolytic fragments were detected by mouse monoclonal anti-phenylalanine hydroxylase IgG<sub>1</sub> (PH8, Calbiochem, 1:2000 dilution) and alkaline phosphatase conjugated anti-mouse IgG (Promega, 1:7500 dilution). Bound antibodies were visualized by chemiluminescence with the CDP-Star substrate (Roche) for alkaline phosphatase. Chemiluminescence was monitored with the DIANA III imaging system, and the resulting protein bands were quantified by AIDA-software (Raytest). The densitometry data of quadruplicate assays of one protein purification were normalized to the band corresponding to intact MBP-PAH fusion protein and analyzed by nonlinear curve fitting of single exponential function in the case of the fusion protein. The formation of the PAH fragment upon cleavage of the fusion protein and subsequent degradation of the PAH fragment was determined by nonlinear curve fitting of a double exponential “Bateman function”:

$$Y = C \times \frac{K_i}{K_i - K_e} \times (e^{-K_e \times t} - e^{-K_i \times t})$$

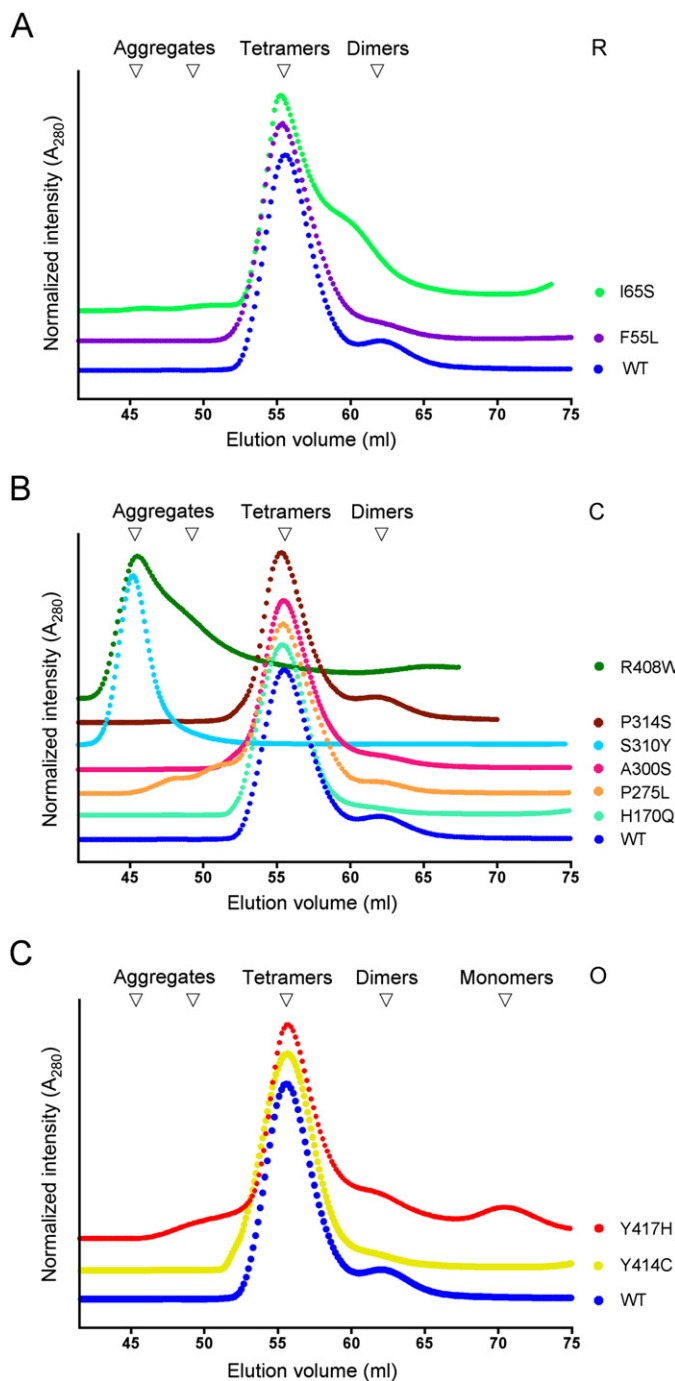
in which  $Y$  is the amount of the PAH protein;  $C$  is the theoretical amount of the MBP-PAH fusion protein;  $K_i$  and  $K_e$  are the rate constants for invasion and elimination of the PAH fragment, respectively; and  $t$  is the incubation time.

### Thermal Inactivation

Thermal inactivation of wild-type and variant MBP-PAH was determined by analysis of the decay of enzyme activity as a function of temperature. Aliquots of protein (1 μg/μl) were incubated in 20 mM Na HEPES, 200 mM NaCl, pH 7.0 for 10 min at 22 different temperatures ranging from 20°C to 75°C and then chilled on ice. PAH enzyme activity was subsequently measured as described above. Residual activities were normalized to initial enzyme activity without incubation. Data points were subjected to nonlinear regression analysis, and midpoints of thermal inactivation ( $T_m$ ) at 50% residual activity observed in three independent experiments were calculated with the use of GraphPad Prism 4.0c with the Boltzmann sigmoidal fit (GraphPad Software).

### Thermal Denaturation

Fluorescence measurements were performed on a Cary Eclipse fluorescence spectrophotometer equipped with a temperature-controlled Peltier multicell holder (Varian). Samples contained MBP-PAH fusion proteins (6 μM PAH subunit) in 20 mM Na HEPES, 200 mM NaCl, pH 7.0, 10 μM ferrous ammonium sulfate, and 1 mM DTT. Thermal denaturation was monitored by the following of changes in 8-anilino-1-naphthalenesulfonic acid (ANS; Sigma Aldrich)-fluorescence emission (excitation at 395 nm and emission at 500 nm, 5.0/10.0 nm slit widths). Thermal denaturation was performed at a rate of 1.2°C/min in a 25°–85°C range. Thermal denaturation curves were obtained by the plotting of fluorescence intensities against temperature. The phase transitions observed in three independent experiments were determined, and the respective transition midpoints were calculated by differentiation of the increasing part of the curves. Significances for the differences between the wild-type and the variants were calculated by two-tailed Student's  $t$  test. Thermal denaturation of the MBP protein occurs at temperatures above 62°C, as previously shown<sup>30</sup> and confirmed for this experimental setup. Therefore, MBP



denaturation did not interfere with the unfolding curves of the PAH protein for ANS fluorescence.

### Structural Analyses and Figure Preparation

A composite model of the 3D structure (PDB codes 1PAH, 1PHZ, 2PHM, 2PAH, 3PAH, 1J8T, and 1J8U) of tetrameric PAH was constructed with the use of the DeepView/Swiss-PdbViewer.<sup>31</sup> In the presence of hydrogen atoms, H bonds were computed with the following constraints: 1.2–2.76 Å distance, 120° angles. When hydrogen atoms were absent, H bonds were computed with the following constraints: 2.35–3.2 Å distance, 90° angles. Figures were prepared with the use of Visual Molecular Dynamics software.<sup>32</sup>

### Figure 2. PAH Mutations in All Three Domains Can Lead to Aggregation or Impaired Tetramer Assembly

Oligomerization profiles of wild-type and variant PAH were determined by size-exclusion chromatography. Chromatograms of variant PAH were normalized to the tetramer peak of the wild-type. Arrows mark the elution volumes of soluble aggregates (45 to 47 ml), tetramers (56 ml), dimers (63 ml), and monomers (71 ml).

(A) Profiles of variants arising from mutations located in the regulatory domain (R). I65S showed increased amounts of dimers, whereas F55L was almost exclusively eluted as tetramers.

(B) Profiles of variants arising from mutations located in the catalytic domain (C). S310Y and R408W eluted as high-molecular-weight aggregates without any detectable tetramers. The variants H170Q, P275L, A300S, and P314S eluted mainly in the tetrameric form. For P275L, two additional peaks of higher molecular weight were detected.

(C) Profiles of variants arising from mutations mapping to the dimerization motif of the oligomerization domain (O). Y417H showed significant amounts of monomers and increased amounts of dimers, whereas Y414C showed only tetramers.

## Results

### Disturbed Oligomerization Manifests as Aggregation or Impaired Tetramer Assembly

Wild-type PAH and ten variant forms of PAH were purified by affinity chromatography with subsequent size-exclusion chromatography, and oligomeric states were quantified by deconvolution analysis (Figure 2 and Table 1). Wild-type PAH was eluted mainly in the tetrameric form (86.2%), with a small amount of dimers (13.8%). Five variant PAH proteins (F55L, H170Q, A300S, P314S, Y414C) that mapped to all three domains showed elution profiles similar to that of wild-type with minor changes of the dimer-tetramer equilibrium. The remaining variants displayed disturbed oligomerization, with only one mutant residue (Y417H) mapping to the oligomerization domain. Impaired tetramer assembly was observed for the I65S mutation located in the regulatory domain and the Y417H mutation located in the dimerization motif of the oligomerization domain. The I65S mutation showed increased amounts of dimers (28.5%). This is in line with previously reported observations for the I65T substitution showing a shifted equilibrium of tetramers and dimers and proneness to aggregation.<sup>18,33,34</sup> For the Y417H variant we observed an oligomerization profile previously not described for recombinant variant PAH. We detected a significant amount of monomers (11.1%), with an increased amount of dimers (17.7%) in relation to tetramers (63.7%), and some aggregates (7.5%). Although the residue Y414 is in close proximity to Y417, the variant Y414C showed an oligomerization pattern resembling that of the wild-type protein. This is in contrast to previous studies that reported aggregate formation for Y414C.<sup>35</sup> Two mutations located in the catalytic domain (S310Y,

**Table 1. Quantitative Analysis of Wild-Type and Variant PAH Oligomerization Profiles**

Missense Mutation	Aggregates	Tetramers	Dimers	Monomers
WT		86.2	13.8	
F55L		94.1	5.9	
I65S		71.5	28.5	
H170Q		94.8	5.2	
P275L	13.2	82.2	4.6	
A300S	2.4	87.0	10.6	
S310Y	100			
P314S		83.2	16.8	
R408W	100			
Y414C		92.5	7.5	
Y417H	7.5	63.7	17.7	11.1

Relative amounts of the eluted fractions corresponding to different oligomeric states of wild-type (WT) and variant PAH proteins are given as percentages. The relative amounts were calculated by deconvolution analysis of the size-exclusion chromatograms.

R408W) resulted in formation of high-molecular-weight aggregates (100%) without the occurrence of any tetrameric PAH, suggesting a severe folding defect. In addition, the variant P275L also formed some aggregates (13.2%), of which the largest fraction (82.2%) was the tetrameric form.

In summary, we observed disturbed oligomerization not only for mutations located in the oligomerization domain but also for mutations located in the two other domains. Our results confirm that PAH mutations can lead to misfolding, with aggregation and/or disturbed tetramer assembly.

### Residual Enzyme Activity of Variant PAH is High, but Allostery is Disturbed

Detailed analyses of steady-state kinetic parameters were performed for all purified tetrameric PAH proteins (Table 2). Enzyme activity of variant PAH was reduced in comparison to wild-type with respect to  $V_{\max}$  determined at variable L-Phe concentrations. However, the reduction in activity was generally moderate ( $\geq 50\%$  residual activity), with the exception of P314S (22% residual activity). For most of the variant proteins analyzed, the affinity of variant PAH to its cofactor BH<sub>4</sub> or to its substrate L-Phe was not reduced. Only P275L showed decreased cofactor affinity, with a threefold increase in  $K_m$  (65  $\mu$ M). By contrast, the  $K_m$  values for A300S (17  $\mu$ M) and Y414C (16  $\mu$ M) were slightly decreased. The affinity to the substrate was not reduced but was even increased for P275L and P314S, as shown by decreased values for  $S_{0.5}$  (76 and 49  $\mu$ M, respectively).

Tetrameric wild-type PAH displayed positive cooperativity for L-Phe binding (Hill coefficient [ $h$ ], 3.0) and substrate activation (activation fold, 3.0). Notably, all but one of the PAH variants showed alterations in allostery. Positive cooperativity was reduced for all variant proteins except H170Q. Most variants showed reduced substrate activation, ranging from a mild decrease (P275L and Y414C; activation fold 2.3 and 2.0, respectively) to a near-complete loss (F55L, I65S, P314S, and Y417H; activation fold 1.5, 1.0, 1.3, and 1.5, respectively).

Taken together, the results show that reduction in enzyme activity was moderate for most variant PAH proteins, and only one variant showed reduced affinity to the cofactor. However, allostery was severely affected by mutations in all three domains. This indicates that side-chain replacements can induce global conformational changes, with remote effects on PAH enzyme function.

### Susceptibility to Proteinase K is Increased

Misfolded subunits and incorrectly assembled oligomeric forms of proteins are more susceptible to degradation by proteases in mammalian cells.<sup>5</sup> Previous studies using a transcription and translation system or the protease trypsin showed that mutations in the PAH gene can lead to decreased protein stability.<sup>3-5,18</sup>

In this study, we probed protein conformation of PAH by limited proteolysis with proteinase K. Here, the proteolytic event is predominantly governed by the stereochemistry and flexibility of the protein substrate and not by the specificity of the protease.<sup>36</sup> Because MBP was fused to the N-terminal regulatory domain of PAH, we hypothesized that altered folding of this domain could lead to increased susceptibility of the linker region to proteolytic cleavage. This was confirmed by the finding that the half-life of the fusion protein was decreased by  $\geq 50\%$  for six out of eight MBP-PAH variants. Stability of the PAH fragment was also decreased in most cases (Table 3). Mutations in the regulatory domain and the oligomerization domain led to minor reductions of PAH half-life, whereas severe destabilization was detected for three mutations of the catalytic domain (H170Q, P275L, A300S; 60%, 55%, and 50% of the wild-type, respectively). Interestingly, one catalytic mutation (P314S) did not lead to destabilization but even induced marked stabilization of both the fusion protein (167%) and the PAH fragment (143%) in comparison to that of the wild-type.

The increased susceptibility to proteinase K observed here is in line with the hypothesis that PAH destabilization is due to partial protein unfolding.

### Protein Unfolding Predominantly Affects the Regulatory Domain of the Protein

To directly investigate whether variant PAH is prone to aberrant folding, we analyzed conformational alterations in the ground state and upon thermal denaturation. Two distinct transitions were previously described for the denaturation of wild-type PAH. These form the basis for a three-stage model of thermal PAH denaturation: (i) a low-temperature transition representing unfolding of the four regulatory domains, (ii) a high-temperature transition representing unfolding of two catalytic domains, and (iii) irreversible protein denaturation.<sup>37</sup>

Thermal protein denaturation was analyzed by ANS fluorescence (Figures 3A, 3B, and 3C). Transition midpoints are summarized in Table 4. The usage of the hydrophobic fluorophore ANS allowed us to monitor overall unfolding events because it binds to hydrophobic groups of the denaturing

**Table 2. Enzyme Kinetic Parameters**

Missense Mutation	L-Phe <sup>a</sup>			BH <sub>4</sub> <sup>b</sup>		
	V <sub>max</sub> <sup>e</sup> (nmol L-Tyr/min × mg protein)	[S] <sub>0.5</sub> <sup>e</sup> (μM)	<i>h</i>	Activation Fold	V <sub>max</sub> <sup>e</sup> (nmol L-Tyr/min × mg protein)	K <sub>m</sub> <sup>e</sup> (μM)
WT	3470 ± 75	155 ± 6	3.0	3.0	3425 ± 139	24 ± 3
F55L	2088 ± 66	128 ± 9	1.5	1.5	2408 ± 112	22 ± 3
I65S	2214 ± 130	168 ± 20	1.4	1.0	3762 ± 152	29 ± 3
H170Q	2174 ± 37	125 ± 4	3.1	3.6	2197 ± 43	25 ± 2
P275L	1706 ± 25	76 ± 3	1.6	2.3	3216 ± 67	65 ± 4
A300S	2990 ± 64	148 ± 6	2.4	3.7	3320 ± 58	17 ± 2
P314S <sup>c</sup>	780 ± 22	49 ± 2	1.9	1.3	760 ± 39	25 ± 4
Y414C <sup>d</sup>	1877 ± 51	104 ± 40	2.2	2.0	1870 ± 50	16 ± 2
Y417H <sup>d</sup>	2258 ± 54	135 ± 40	2.5	1.5	2866 ± 188	31 ± 4

Steady-state kinetic parameters of wild-type (WT) and variant tetrameric MBP-PAH fusion proteins. Activation fold represents the substrate activation as the ratio of specific activity with and without prior incubation with L-Phe. Apparent affinities for L-Phe ([S]<sub>0.5</sub>) and BH<sub>4</sub> (K<sub>m</sub>) and the Hill-coefficient (*h*) as a measure of cooperativity are shown.

<sup>a</sup> Enzyme kinetic parameters determined at variable L-Phe concentrations and standard BH<sub>4</sub> concentration in three independent experiments.

<sup>b</sup> Enzyme kinetic parameters determined at variable BH<sub>4</sub> concentrations and standard L-Phe concentration in three independent experiments.

<sup>c</sup> L-Phe concentrations restricted to 0–250 μM.

<sup>d</sup> L-Phe concentrations restricted to 0–500 μM.

<sup>e</sup> Values are given as means ± SEM.

protein and shows a high quantum yield in its bound state but not when solved in aqueous buffers.<sup>38</sup> ANS-fluorescence analysis of tetrameric wild-type PAH fusion proteins revealed a low-temperature transition and a high-temperature transition, with their respective midpoints at 47.3°C and 55.0°C. This is in agreement with previous results obtained by differential scanning calorimetry.<sup>37</sup>

The two mutations located in the regulatory domain (F55L, I65S) induced alterations in unfolding patterns. An elevated fluorescence signal for I65S in comparison to wild-type was detected in the ground state at 25°C. This indicates an increased hydrophobicity due to partial protein unfolding. The same was true to a minor extent for F55L.

**Table 3. Proteolytic Stability of Wild-Type and Variant PAH**

Missense Mutation	t <sub>1/2</sub> FP			t <sub>1/2</sub> PAH		
	(% of WT)	SEM	p Value	(% of WT)	SEM	p Value
WT	100			100		
F55L	71	7	0.039	75	15	ns
I65S	34	7	0.001	85	17	ns
H170Q	26	5	0.001	60	12	0.003
P275L	40	4	0.001	55	16	0.002
A300S	31	9	0.001	50	16	0.001
P314S	167	10	0.013	143	16	0.019
Y414C	47	13	0.004	70	16	0.017
Y417H	52	4	0.003	86	18	ns

Stability of wild-type (WT) and variant PAH against limited proteolysis by proteinase K. Degradation of the MBP-PAH fusion protein and formation with subsequent degradation of the PAH fragment were probed by western-blotting analyses. Densitometry data were normalized to intact MBP-PAH fusion protein and the resulting data points were fitted by single exponential function (MBP-PAH fusion proteins) and by double exponential Bateman function (PAH fragment). The calculated half-lives of fusion proteins (t<sub>1/2</sub> FP) and of PAH fragments (t<sub>1/2</sub> PAH) are given in percent ± SEM of *n* = 4 independent experiments. Significances for the differences between wild-type and the variants were calculated by two-tailed Student's *t* test.

During thermal unfolding, F55L showed a left-shift of the low-temperature transition in comparison with the wild-type protein (t<sub>m1/2</sub> 43.7°C), whereas a complete loss of the low-temperature transition was observed for I65S. By contrast, neither F55L nor I65S significantly affected the high-temperature transition. These findings indicate that the two mutations located in the regulatory domain induced misfolding and facilitated unfolding of the respective domain but did not influence the conformational stability of the catalytic domain.

Thermal unfolding of variant PAH was also affected by the four mutations located in the catalytic domain. All variants but P275L showed elevated ground-state levels of ANS fluorescence. All residue substitutions in the catalytic domain induced a left-shift of the low-temperature transition that reached statistical significance for A300S (t<sub>m1/2</sub> 44.6°C) and P275L (t<sub>m1/2</sub> 44.1°C). Interestingly, none of the mutations located in the catalytic domain significantly altered the high-temperature transition, indicating that these mutations did not affect unfolding of the catalytic domain itself but induced a loss of structural integrity of the regulatory domain.

Distinct alterations of thermal-unfolding parameters were observed for the two mutations located in the oligomerization domain (Y414C, Y417H). In contrast to other variants exhibiting accelerated thermal unfolding, the ground-state ANS fluorescence of Y414C and Y417H remained unchanged. However, the low-temperature transition was considerably left-shifted for Y414C (t<sub>m1/2</sub> 43.1°C) and for Y417H (t<sub>m1/2</sub> 41.9°C), whereas no effect on the high-temperature transition was detected. The residues Y414 and Y417 are located close to the site of interaction between the oligomerization domain and the regulatory domain within one PAH subunit. This might explain the effect of these side-chain replacements on the stability of the regulatory domain.

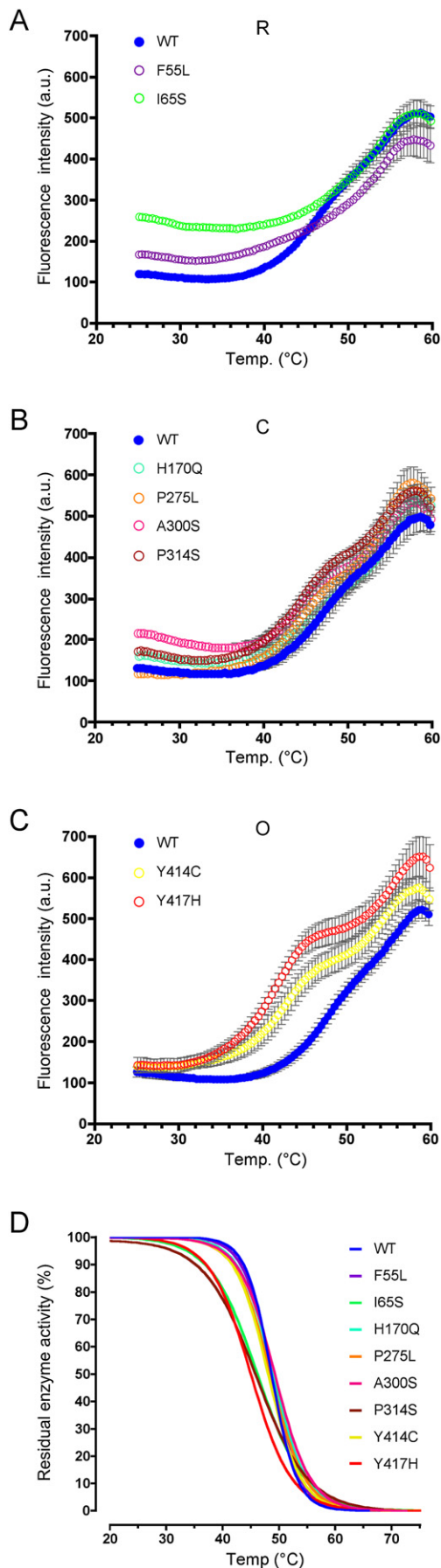


### Figure 3. PAH Mutations Lead to Accelerated Thermal Unfolding and Early Thermal Inactivation for Some Variants

(A–C) Thermal-unfolding profiles of wild-type and variant PAH monitored by ANS fluorescence. Intensities of the fluorescent dye ANS, which binds to hydrophobic groups of the protein presented upon unfolding, are plotted as a function of increasing temperatures. Error bars represent the mean  $\pm$  SEM of three independent experiments. The resulting denaturation curves consist of three segments: a native baseline and two partially overlapping phase transitions corresponding to unfolding of the regulatory domain (first transition) and of the catalytic domain (second transition), respectively. Ground-state ANS fluorescence was markedly elevated for I65S and A300S, indicating increased protein areas available for dye binding. I65S lacked the first transition; all other variants showed a left-shift of the first transition, indicating a destabilization of the regulatory domain in comparison to the wild-type. The second transition was not affected. R denotes regulatory domain; C denotes catalytic domain; O denotes oligomerization domain.

(D) Time course of thermal inactivation of wild-type and variant PAH. Proteins were incubated at increasing temperatures, and the residual enzyme activities were determined. Data points of residual activities were normalized to the initial enzyme activity and subjected to nonlinear regression analysis. For three variants that mapped to all domains (I65S, P314S, and Y417H), curves were left-shifted in comparison to the wild-type. The remaining five variants showed inactivation profiles comparable to that of wild-type PAH.

To assess the impact of thermal stress on PAH enzyme activity, we performed thermal-inactivation assays (Figure 3D). A reduction of the thermal-inactivation midpoints at 50% residual activity ( $T_m$ ) in comparison to the wild-type protein (48.8°C) was observed for three variants (I65S, P314S, Y417H,  $T_m$ ; 46.2, 44.5, and 45.0°C, respectively), whereas thermal inactivation of the other variants was not altered (Table 4). The affected residues mapped to all protein domains, demonstrating that mutations located outside the catalytic domain can also disturb enzyme function.

In summary, the results of thermal denaturation show that mutations in the PAH gene lead to substantial distortion of the protein's conformation, with particular impact on the regulatory domain.

### Local Amino Acid Replacements Can Affect Networks of Amino Acid Interactions

We constructed a composite 3D model of the full-length PAH tetramer and performed 3D structural modeling. Side-chain interactions in the local environment of amino acid residues affected by mutations in our patients were analyzed in order to investigate whether these amino acid residues are directly or indirectly involved in networks of side-chain interactions with functional and conformational impact. Our observations indicate that local amino acid replacements can induce global conformational changes, with remote effects on enzyme function and stability of the PAH.

**Table 4. Transition Midpoints and Midpoints of Thermal Inactivation for Thermal Denaturation of Wild-Type and Variant PAH**

Protein Domain Affected	ANS Fluorescence				Thermal Inactivation						
	Missense Mutation	$t_{m1/2}$	SEM	p Value	$t_{m2/3}$	SEM	p Value	Missense Mutation	$T_m$	SEM	p Value
-	WT	47.0	0.03		54.8	0.30		WT	48.85	0.52	
R	F55L	43.7	0.57	0.004	54.5	0.03	ns	F55L	47.96	0.72	ns
R	I65S	-	-	-	53.9	0.30	ns	I65S	46.17	0.56	0.042
-	WT	47.0	0.52		55.1	0.30					
C	H170Q	46.1	0.00	ns	55.4	0.52	ns	H170Q	48.92	0.20	ns
C	P275L	44.1	0.52	0.029	54.6	0.05	ns	P275L	48.40	0.76	ns
C	A300S	44.6	0.30	0.016	54.5	0.03	ns	A300S	49.46	0.61	ns
C	P314S	44.9	0.60	ns	54.5	0.03	ns	P314S	44.50	1.05	0.021
-	WT	47.9	0.52		55.1	0.30					
O	Y414C	43.1	0.30	0.001	54.5	0.03	ns	Y414C	48.42	0.43	ns
O	Y417H	41.9	0.30	0.001	55.4	0.03	ns	Y417H	44.99	0.21	0.011
-	WT (mean)	47.3	0.26		55.0	0.16					

Transition midpoints and midpoints of thermal inactivation obtained by thermal denaturation of wild-type PAH were compared to variants arising from mutations in the regulatory (R), catalytic (C), and the oligomerization (O) domain. For ANS-fluorescence three sets of experiments covering the mutations of different domains were carried out separately. The transition midpoints of the first ( $t_{m1/2}$ ) and the second transitions ( $t_{m2/3}$ ) were calculated by differentiation of the increasing part of the curves and are given in °C as means  $\pm$  SEM of  $n = 3$  independent experiments. For thermal inactivation residual activities were subjected to nonlinear regression analysis and the midpoints of thermal inactivation ( $T_m$ ) were calculated.  $T_m$ -values representing the temperature at 50% residual activity are given in °C as means  $\pm$  SEM of quadruplicate assays in  $n = 2$  independent experiments. Significances for the differences between wild-type and the variants were calculated by two-tailed Student's *t* test.

F55 and I65 are part of the hydrophobic core of the regulatory domain. Whereas F55L showed no impact on tetramer assembly, I65S displayed disturbed oligomerization, with increased amounts of dimeric protein in comparison to the wild-type (Figure 2). The assembly of dimers to tetrameric PAH is promoted by coiled-coil interactions of the C-terminal  $\alpha$  helices,<sup>7</sup> which are preceded by two antiparallel strands forming a  $\beta$  ribbon that comprises the dimerization motif (residues 411–427).<sup>15,17</sup> This  $\beta$  ribbon interacts with the regulatory domain in the same subunit and with the catalytic domain in the adjacent subunit within the dimer (Figures 4A–4D). The electrostatic interactions of D415 and E422 with R71 located in the prominent loop 68–75 play a pivotal role for the proper position of the dimerization motif, resulting in the right orientation of the  $\alpha$ -helical tetramerization motif for correct tetramer assembly. A distortion of the hydrophobic packing in the regulatory domain due to a substitution of the hydrophobic isoleucine by the polar serine at position 65 is supposed to lead to a displacement of the loop 68–75.<sup>10</sup> Hence, an alteration of the interaction of this loop with the dimerization motif might lead to dislocation of the  $\alpha$ -helical tetramerization motif and result in altered oligomerization with increased amounts of dimers.

Two of the PAH variants located in the catalytic domain (S310Y and R408W) were exclusively purified as high-molecular-weight aggregates lacking all residual enzyme activity (Table 1 and Figure 2). Formation of aggregates was previously described for R408W and structurally explained by potential disruption of hydrogen bonding to L308 and L311.<sup>7,8</sup> The S310 residue builds a hydrogen bond to G307, which interacts with L311. We thus inferred that both S310 and R408 are part of a hydrogen-bonding network formed by G307, L308, S310, L311, and R408 (Figures 4B

and 4C). The R408 residue is located between two proline residues, which define a sharp turn preceding the dimerization motif. This hinge region anchors the oligomerization domain to the catalytic domain and thereby ensures its proper orientation. A disruption of the network by the nonconservative substitutions S310Y and R408W could therefore well induce severe distortion of the protein's oligomeric state.

P314 adopts a central position in a network that comprises residues of the regulatory and the catalytic domain (Figure 4C). There is only one direct interaction between the backbone carbonyl of P314 and the backbone amide of Y317. However, the P314 residue is located in a loop (residues 311–314) connecting  $\alpha$  helices C $\alpha$ 8 and C $\alpha$ 9 that define the active site. The neighboring residues D315 and A313 form a network of interactions with R252 near the pterin-binding loop (residues 248–251), with K113 in the regulatory domain, and with D27 in the autoregulatory sequence. Thus, local changes of the protein conformation in the neighborhood of P314 could induce structural changes at the active site, at the pterin-binding site, and in the regulatory domain. This is in line with the observation that the variant P314S affected various enzyme kinetic parameters with low residual activity, loss of activation, and reduced cooperativity.

Y414C and Y417H, the variants arising from mutations mapping to the oligomerization domain, surprisingly exhibited clearly different oligomerization patterns although they are located in close proximity to each other. Both residues are part of the dimerization motif (Figure 4D). Y414 interacts with the catalytic domain of the same subunit, whereas Y417 is located at the interface of monomer-monomer interactions in the dimer, where it builds a network with T238, R261, and Q304 of the adjacent subunit.

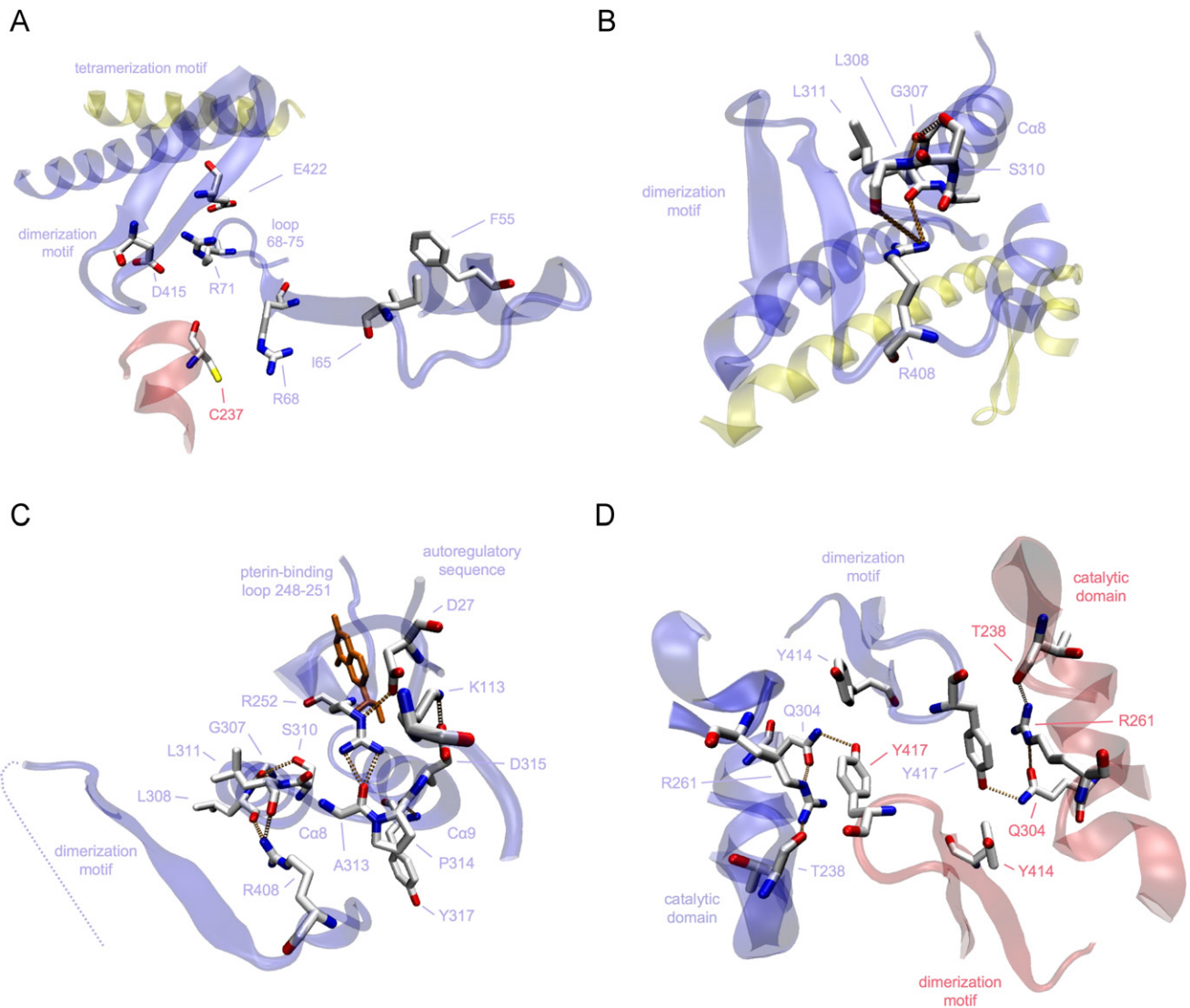


**Figure 4. Amino Acid Residues Affected by PAH Mutations Are Involved in Functional Networks of Side-Chain Interactions**

Selected parts of subunit backbones are shown as ribbon representations, and selected residues are depicted as stick models with carbon atoms in white, oxygen atoms in red, and nitrogen atoms in blue. Hydrogen bonds are shown as golden dotted lines.

(A) Residues F55 and I65 are located in the hydrophobic core of the regulatory domain (subunit A, blue) followed by the prominent loop 68–75. Upon substrate activation, R68 builds a hydrogen bond to C237 in the catalytic domain of the adjacent monomer (subunit D, red). R71 establishes electrostatic interactions with D415 and E422 in the dimerization motif, followed by coiled-coil interaction of the tetramerization motif with the adjacent dimer (subunit B, yellow). The electrostatic interactions are supposed to hold the  $\beta$ -ribbon in its proper spatial position resulting in the right orientation of the  $\alpha$ -helical tetramerization motif.

(B) Residues S310 and R408 are both part of a hydrogen-bonding network that anchors the entire oligomerization domain to the catalytic domain within one subunit. The coiled-coil interaction of subunits A (blue) and B (yellow) of both dimers contributes to tetramer assembly. R408 builds hydrogen bonds to the main-chain carbonyl oxygens of L308 and L311 located in the active-site helix  $C\alpha 8$ . S310 contributes to this network through interaction with G307 that builds a hydrogen bond to the main-chain amide of L311.

(C) P314 is part of the loop 311–314 connecting  $\alpha$  helices  $C\alpha 8$  and  $C\alpha 9$  that define the bottom of the active site. The network of R252, A313, P314, D315, and Y317 contributes to the correct spatial orientation of the active site and the pterin-binding loop 248–251. It is expanded via interaction with residues D27, located in the intrinsic autoregulatory sequence (1–33), and K113, located in a hinge-bending region (111–117) connecting the catalytic to the regulatory domain. This area is in close proximity to the network comprising residues S310 and R408 (B), which constitutes the connection of the whole region with the dimerization motif of the oligomerization domain.  $BH_4$  at the active site is shown as an orange stick model.

(D) Y414 and Y417 are located in a loop connecting two antiparallel  $\beta$  strands forming the dimerization motif. Y417 joins a network comprising residues Q304, R261, and T238, which tightly links the dimerization motif to the catalytic domain of the adjacent subunit (subunit A, blue; subunit D, red). The hydroxyl group of Y417 builds a hydrogen bond to Q304, and the aromatic ring of Y417 stacks with the positively charged guanidinium group of R261. Q304 and T238 are connected to R261 via hydrogen bonds. Y414 is localized in close proximity to residue Y417 but does not contribute to the monomer-monomer interaction.

Y417H is supposed to disrupt the hydrogen bond to Q304 and to damage the polar  $\pi$  stacking due to repulsions between the histidine and the positively charged guanidinium group of R261. This would result in hindrance of dimer formation with the appearance of monomers, and, as a consequence, disturbed tetramerization.

Taken together, the results of the *in silico* structural analysis of this subset of variants support the notion that local replacement of an amino acid at one site can disturb amino acid networks and, as a consequence, induce global changes in conformation that also affect remote parts of the protein at the functional level.

## Discussion

Despite the severe clinical phenotype of PKU, many missense mutations in the *PAH* gene have previously been shown to be associated with surprisingly high residual enzyme activities *in vitro*. It therefore has to be anticipated that mutations lead to loss of function through mechanisms other than impaired catalysis. Previous studies reported on *PAH* protein aggregation and rapid degradation,<sup>3,4,18,39</sup> raising the hypothesis that aberrant folding is a consequence of *PAH* mutations. Recent work substantiated this hypothesis, providing predictions about the effect of *PAH* mutations on native-state-protein stability.<sup>23</sup> Here, we present several lines of experimental evidence that support the hypothesis that *PAH* missense mutations associated with the newly recognized clinical phenotype of BH<sub>4</sub>-responsive *PAH* deficiency lead to protein misfolding. Two mutations (S310Y and R408W) caused severe structural distortion, with protein aggregation and complete loss of enzyme function. The others showed milder alterations of conformation but were associated with impaired enzyme-kinetic parameters, oligomerization, and protein stability at different degrees. Moreover, we showed that *PAH* mutations not only have an impact on the local structural environment of the affected side chain but rather induce alterations consistent with distortion of the enzyme's global conformation.

Interestingly, all variant *PAH* proteins analyzed in our study showed disturbed regulation. Allostery in general and *PAH* allostery in particular are complex events in which numerous side-chain interactions transmit structural changes throughout the whole oligomer. Extensive previous work has defined specific sites that are involved in *PAH* allostery.<sup>12,15,34</sup> Allosteric conformational changes in substrate binding result not only in positive cooperativity but also in activation of the enzyme. We observed that all but one variant led to reduced cooperativity, and six mutations that mapped to all three domains induced a loss of substrate activation. This led us to assume that mutations affecting sites involved in allostery cause a cascade of structural consequences, with alteration of conformational flexibility. As a result, remote functional units of side-chain interactions could be disturbed. Indeed, we ob-

served a negative impact of the I65S mutation located in the regulatory domain on the tetramer-dimer equilibrium. On a structural level, this can be explained by the multiple interactions required for *PAH* oligomerization that are not limited to the oligomerization domains but also involve allosteric contacts of all domains.

Additional evidence for protein misfolding arose from results demonstrating destabilization of variant *PAH* against proteolytic attack by proteinase K. In general, misfolded or partly unfolded proteins show enhanced backbone flexibility and thus facilitate proteolytic attack.<sup>36</sup> Results from limited proteolysis pointed to altered folding of the N-terminal regulatory domain. Moreover, mutations located on the protein surface (H170Q, P275L) were shown to be particularly prone to proteolytic attack, whereas mutations buried in the core of the protein (F55L, I65S, Y417H) were not. Direct experimental evidence for alterations in global protein conformation arose from the analysis of *PAH* hydrophobicity in the ground state and during thermal denaturation. Presentation of hydrophobic groups at the variant protein's surface caused by protein misfolding facilitates binding of the ANS fluorophore. Indeed, an increase in ANS fluorescence in the ground state was observed for the two mutations in the regulatory domain and for most mutations in the catalytic domain. Interestingly, all variant *PAH* showed accelerated thermal unfolding. Furthermore, our investigations revealed that independent of the position of the affected residue, *PAH* mutations had the most impact on the unfolding of the regulatory domain. This was confirmed by analysis of the inactivation of enzyme function by thermal stress. Only three mutations led to accelerated thermal inactivation (I65S, P314S, Y417H); among these, just one mapped to the catalytic domain. Altogether, data from stability assays indicate that the structural conformation of the *PAH* regulatory domain is particularly unstable. This observation can be explained by the structural characteristics of this domain. Recently, Liberles et al. provided strong evidence that the regulatory domain of *PAH* comprises an evolutionary mobile regulatory module, the ACT domain.<sup>12</sup> It facilitates allosteric regulation via transmission of finely tuned conformational changes, a process that appears to be set by the regulatory domains' interactions with the partner domains. These interactions require a high degree of conformational flexibility. For *PAH* isolated from a cold-adapted organism, it was shown that an increase in conformational flexibility is accompanied by an increase in thermostability.<sup>40</sup> Thus, the mobility of the regulatory domain that allows for complex regulation of activity and the oligomeric state might on the other hand cause reduced stability against thermal stress and proteolytic attack. Moreover, the extensive networking of the regulatory domain with other parts of the protein could account for the adoption of misfolding from remote sites. By contrast, missense mutations, if not structurally disruptive, hardly affected the integrity of the catalytic domain. This was shown by unchanged patterns of thermal unfolding of the catalytic

domain and further supported by the variant's high residual enzyme activity and minor changes in thermal-inactivation experiments. The domain's dense tertiary structure with few flexible regions could be the reason for these observations.

Taken together, the results presented here indicate that *PAH* missense mutations can lead to protein misfolding and conformational destabilization at different degrees. Our findings are in agreement with recent results from computational analyses using the FoldX algorithm. This study showed that a significant share of a large set of *PAH* mutations is predicted to provoke protein misfolding. Moreover, the authors raised the hypothesis that residues buried in the 3D structure, unlike those in flexible regions, are particularly prone to severe misfolding.<sup>23</sup> Our findings confirm this at the experimental level for a subset of ten mutations identified in patients with BH<sub>4</sub>-responsive *PAH* deficiency. Mutations at the center of the protein structure (S310Y, R408W) were shown to lead to severe aggregation and complete disruption of structural integrity. Conversely, mutations in flexible regions of the protein (H170Q, P275L, P314S, Y417H) did not primarily show severe protein misfolding. However, they can indeed cause milder conformational changes, which still exert deleterious effects on enzyme function. Features like oligomerization, allostery, activation, and cooperativity need complex conformational rearrangements, which are communicated through flexible regions of the protein via networks of amino acid interactions. Our observations imply that mutations, even those in flexible protein regions, can severely affect enzyme function and stability if they directly or indirectly disrupt these networks. In addition to our results from naturally occurring mutations, this was previously shown by analysis of artificial mutations of amino acid residues in flexible hinge-bending regions. These are involved in substrate-triggered molecular motions, and the corresponding proteins showed a reduced conformational stability in comparison to that of wild-type *PAH*.<sup>13</sup> Finally, two observations exemplify that there also appears to be no general rule for missense mutations of buried residues leading to severe misfolding with protein destabilization and impaired enzyme function. Both A300 and P314 are located in the active center of the protein; A300 is part of helix C $\alpha$ 8, which together with helix C $\alpha$ 9 defines the catalytic core, whereas P314 lies in a flexible loop between helices C $\alpha$ 8 and C $\alpha$ 9. A300S led to conformational destabilization, with distinct proneness to proteinase K and elevated ground-state ANS fluorescence. Nonetheless, enzyme function remained virtually unaffected. Conversely, P314S showing a clear stabilization toward proteinase K led to a marked reduction in enzyme activity and to accelerated thermal inactivation.

The results from our experimental work revealed that *PAH* misfolding is probably communicated throughout the protein by disruption of functionally crucial networks of amino acid interactions. Thus, the classical domain-associated view of mutational effects on the protein might

be insufficient for understanding of the molecular phenotype, and it disregards the well-known complexity in structure and regulation of the *PAH* protein.<sup>15,37</sup> We therefore propose a view of *PAH* that not only considers three primary-structure domains but takes into account that the *PAH* enzyme is an entity of functional units that arise from the tertiary and quaternary protein structure. If this holds true, mutations in the *PAH* gene exert their effects by disturbance of these functional units.

PKU has evolved from a model of a genetic disease that leads to severe neurologic impairment to a model of a treatable protein-folding disease with loss of function. The new insights into molecular mechanisms of protein misfolding are a prerequisite for the unraveling of how the natural cofactor BH<sub>4</sub> corrects the biochemical consequences of *PAH* gene mutations and will help treatment of patients on an individually tailored basis.

### Supplemental Data

One supplemental table is available with this article online at <http://www.ajhg.org/>.

### Acknowledgments

This work was supported by the Bavarian Genome Research Network (BayGene). We are indebted to our patients and to their families; to Eduard Manzinger for generating the expression clones; to Susi Wullinger for excellent technical assistance; to Doris Bruer for genotyping; to Esther M Maier for important discussions; and to Dietrich Reinhardt for continuous support. This article is part of an M.D. thesis to be submitted by M.S. and of Ph.D. theses to be submitted by D.D.M. and by M.K.D.

Received: February 19, 2008

Revised: May 9, 2008

Accepted: May 17, 2008

Published online: June 5, 2008

### Web Resources

The URLs for data presented herein are as follows:

BIOPKU: International Database of Patients and Mutations causing BH<sub>4</sub>-responsive HPA/PKU, <http://www.bh4.org/biopku.html>

Online Mendelian Inheritance in Man (OMIM), <http://www.ncbi.nlm.nih.gov/Omim/>

PAHdb, <http://www.pahdb.mcgill.ca/>

PDB, <http://www.rcsb.org/pdb/>

### References

1. Scriver, C.R. (2007). The *PAH* gene, phenylketonuria, and a paradigm shift. *Hum. Mutat.* 28, 831–845.
2. Muntau, A.C., Röschinger, W., Habich, M., Demmelmair, H., Hoffmann, B., Sommerhoff, C.P., and Roscher, A.A. (2002). Tetrahydrobiopterin as an alternative treatment for mild phenylketonuria. *N. Engl. J. Med.* 347, 2122–2132.

3. Erlandsen, H., Pey, A.L., Gámez, A., Pérez, B., Desviat, L.R., Aguado, C., Koch, R., Surendran, S., Tyring, S., Matalon, R., et al. (2004). Correction of kinetic and stability defects by tetrahydrobiopterin in phenylketonuria patients with certain phenylalanine hydroxylase mutations. *Proc. Natl. Acad. Sci. USA* *101*, 16903–16908.
4. Pey, A.L., Pérez, B., Desviat, L.R., Martínez, M.A., Aguado, C., Erlandsen, H., Gámez, A., Stevens, R.C., Thóroflsson, M., Ugarte, M., et al. (2004). Mechanisms underlying responsiveness to tetrahydrobiopterin in mild phenylketonuria mutations. *Hum. Mutat.* *24*, 388–399.
5. Waters, P.J. (2003). How PAH gene mutations cause hyperphenylalaninemia and why mechanism matters: insights from in vitro expression. *Hum. Mutat.* *21*, 357–369.
6. Kobe, B., Jennings, I.G., House, C.M., Michell, B.J., Goodwill, K.E., Santarsiero, B.D., Stevens, R.C., Cotton, R.G., and Kemp, B.E. (1999). Structural basis of autoregulation of phenylalanine hydroxylase. *Nat. Struct. Biol.* *6*, 442–448.
7. Fusetti, F., Erlandsen, H., Flatmark, T., and Stevens, R.C. (1998). Structure of tetrameric human phenylalanine hydroxylase and its implications for phenylketonuria. *J. Biol. Chem.* *273*, 16962–16967.
8. Erlandsen, H., Fusetti, F., Martínez, A., Hough, E., Flatmark, T., and Stevens, R.C. (1997). Crystal structure of the catalytic domain of human phenylalanine hydroxylase reveals the structural basis for phenylketonuria. *Nat. Struct. Biol.* *4*, 995–1000.
9. Flatmark, T., and Stevens, R.C. (1999). Structural insight into the aromatic amino acid hydroxylases and their disease-related mutant forms. *Chem. Rev.* *99*, 2137–2160.
10. Erlandsen, H., and Stevens, R.C. (1999). The structural basis of phenylketonuria. *Mol. Genet. Metab.* *68*, 103–125.
11. Freimer, N., and Sabatti, C. (2003). The human genome project. *Nat. Genet.* *34*, 15–21.
12. Liberles, J.S., Thóroflsson, M., and Martínez, A. (2005). Allosteric mechanisms in ACT domain containing enzymes involved in amino acid metabolism. *Amino Acids* *28*, 1–12.
13. Stokka, A.J., Carvalho, R.N., Barroso, J.F., and Flatmark, T. (2004). Probing the role of crystallographically defined/predicted hinge-bending regions in the substrate-induced global conformational transition and catalytic activation of human phenylalanine hydroxylase by single-site mutagenesis. *J. Biol. Chem.* *279*, 26571–26580.
14. Andersen, O.A., Stokka, A.J., Flatmark, T., and Hough, E. (2003). 2.0 Å resolution crystal structures of the ternary complexes of human phenylalanine hydroxylase catalytic domain with tetrahydrobiopterin and 3-(2-thienyl)-L-alanine or L-norleucine: substrate specificity and molecular motions related to substrate binding. *J. Mol. Biol.* *333*, 747–757.
15. Thóroflsson, M., Teigen, K., and Martínez, A. (2003). Activation of phenylalanine hydroxylase: effect of substitutions at Arg68 and Cys237. *Biochemistry* *42*, 3419–3428.
16. Bjørge, E., Knappskog, P.M., Martínez, A., Stevens, R.C., and Flatmark, T. (1998). Partial characterization and three-dimensional-structural localization of eight mutations in exon 7 of the human phenylalanine hydroxylase gene associated with phenylketonuria. *Eur. J. Biochem.* *257*, 1–10.
17. Knappskog, P.M., Flatmark, T., Aarden, J.M., Haavik, J., and Martínez, A. (1996). Structure/function relationships in human phenylalanine hydroxylase. Effect of terminal deletions on the oligomerization, activation and cooperativity of substrate binding to the enzyme. *Eur. J. Biochem.* *242*, 813–821.
18. Waters, P.J., Parniak, M.A., Akerman, B.R., and Scriver, C.R. (2000). Characterization of phenylketonuria missense substitutions, distant from the phenylalanine hydroxylase active site, illustrates a paradigm for mechanism and potential modulation of phenotype. *Mol. Genet. Metab.* *69*, 101–110.
19. Waters, P.J., Parniak, M.A., Hewson, A.S., and Scriver, C.R. (1998). Alterations in protein aggregation and degradation due to mild and severe missense mutations (A104D, R157N) in the human phenylalanine hydroxylase gene (PAH). *Hum. Mutat.* *12*, 344–354.
20. Guldberg, P., Rey, F., Zschocke, J., Romano, V., Francois, B., Michiels, L., Ullrich, K., Hoffmann, G.F., Burgard, P., Schmidt, H., et al. (1998). A European multicenter study of phenylalanine hydroxylase deficiency: classification of 105 mutations and a general system for genotype-based prediction of metabolic phenotype. *Am. J. Hum. Genet.* *63*, 71–79.
21. Scriver, C.R. (2006). Preface. In *PKU and BH<sub>4</sub>-Advances in Phenylketonuria and Tetrahydrobiopterin*, N. Blau, ed. (Heilbronn: SPS Verlagsgesellschaft), pp. 23–31.
22. Scriver, C.R., and Waters, P.J. (1999). Monogenic traits are not simple: lessons from phenylketonuria. *Trends Genet.* *15*, 267–272.
23. Pey, A.L., Stricher, F., Serrano, L., and Martínez, A. (2007). Predicted effects of missense mutations on native-state stability account for phenotypic outcome in phenylketonuria, a paradigm of misfolding diseases. *Am. J. Hum. Genet.* *81*, 1006–1024.
24. Solstad, T., and Flatmark, T. (2000). Microheterogeneity of recombinant human phenylalanine hydroxylase as a result of nonenzymatic deamidations of labile amide containing amino acids. Effects on catalytic and stability properties. *Eur. J. Biochem.* *267*, 6302–6310.
25. Martínez, A., Knappskog, P.M., Olafsdottir, S., Døskeland, A.P., Eiken, H.G., Svebak, R.M., Bozzini, M., Apold, J., and Flatmark, T. (1995). Expression of recombinant human phenylalanine hydroxylase as fusion protein in *Escherichia coli* circumvents proteolytic degradation by host cell proteases. Isolation and characterization of the wild-type enzyme. *Biochem. J.* *306*, 589–597.
26. Gámez, A., Perez, B., Ugarte, M., and Desviat, L.R. (2000). Expression analysis of phenylketonuria mutations. Effect on folding and stability of the phenylalanine hydroxylase protein. *J. Biol. Chem.* *275*, 29737–29742.
27. Pey, A.L., and Martinez, A. (2005). The activity of wild-type and mutant phenylalanine hydroxylase and its regulation by phenylalanine and tetrahydrobiopterin at physiological and pathological concentrations: an isothermal titration calorimetry study. *Mol. Genet. Metab.* *86 (Suppl 1)*, S43–S53.
28. Miranda, F.F., Teigen, K., Thóroflsson, M., Svebak, R.M., Knappskog, P.M., Flatmark, T., and Martínez, A. (2002). Phosphorylation and mutations of Ser(16) in human phenylalanine hydroxylase. Kinetic and structural effects. *J. Biol. Chem.* *277*, 40937–40943.
29. Copeland, R.A. (2000). *Enzymes: a practical introduction to structure, mechanism, and data analysis* (New York, Chichester: J. Wiley).
30. Novokhatny, V., and Ingham, K. (1997). Thermodynamics of maltose binding protein unfolding. *Protein Sci.* *6*, 141–146.
31. Guex, N., and Peitsch, M.C. (1997). SWISS-MODEL and the Swiss-PdbViewer: an environment for comparative protein modeling. *Electrophoresis* *18*, 2714–2723.

32. Humphrey, W., Dalke, A., and Schulten, K. (1996). VMD: visual molecular dynamics. *J. Mol. Graph.* *14*, 33–38, 27–28.
33. Nascimento, C., Botelho, H.M., Tavares de Almeida, I., Gomes, C.M., and Leandro, P. (2007). Folding rescue of mild PKU mutations by chemical chaperones. *J. Inherit. Metab. Dis.* *30 (Suppl 1)*, 11.
34. Pey, A.L., Thórolfsson, M., Teigen, K., Ugarte, M., and Martínez, A. (2004). Thermodynamic characterization of the binding of tetrahydropterins to phenylalanine hydroxylase. *J. Am. Chem. Soc.* *126*, 13670–13678.
35. Pey, A.L., Desviat, L.R., Gámez, A., Ugarte, M., and Pérez, B. (2003). Phenylketonuria: genotype-phenotype correlations based on expression analysis of structural and functional mutations in PAH. *Hum. Mutat.* *21*, 370–378.
36. Fontana, A., de Laureto, P.P., Spolaore, B., Frare, E., Picotti, P., and Zambonin, M. (2004). Probing protein structure by limited proteolysis. *Acta Biochim. Pol.* *51*, 299–321.
37. Thórolfsson, M., Ibarra-Molero, B., Fojan, P., Petersen, S.B., Sanchez-Ruiz, J.M., and Martínez, A. (2002). L-phenylalanine binding and domain organization in human phenylalanine hydroxylase: a differential scanning calorimetry study. *Biochemistry* *41*, 7573–7585.
38. Royer, C.A. (1995). Fluorescence spectroscopy. *Methods Mol. Biol.* *40*, 65–89.
39. Pérez, B., Desviat, L.R., Gomez-Puertas, P., Martínez, A., Stevens, R.C., and Ugarte, M. (2005). Kinetic and stability analysis of PKU mutations identified in BH4-responsive patients. *Mol. Genet. Metab.* *86 (Suppl 1)*, S11–S16.
40. Leiros, H.K., Pey, A.L., Innselset, M., Moe, E., Leiros, I., Steen, I.H., and Martínez, A. (2007). Structure of phenylalanine hydroxylase from *Colwellia psychrerythraea* 34H, a monomeric cold active enzyme with local flexibility around the active site and high overall stability. *J. Biol. Chem.* *282*, 21973–21986.